A genome-wide CRISPR screen identifies a restricted set of HIV host dependency factors

Ryan J Park[1–3,20], Tim Wang[3–6,20], Dylan Koundakjian[1], Judd F Hultquist[7,8], Pedro Lamothe-Molina[1,9], Blandine Monel[1,10], Kathrin Schumann[11], Haiyan Yu[3], Kevin M Krupzcak[5], Wilfredo Garcia-Beltran[1,2], Alicja Piechocka-Trocha[1], Nevan J Krogan[7,8], Alexander Marson[11–15], David M Sabatini[3–6,16], Eric S Lander[3,4,17], Nir Hacohen[3,18] & Bruce D Walker[1,3,10,19]

© 2017 Nature America, Inc., part of Springer Nature. All rights reserved.

Host proteins are essential for HIV entry and replication and can be important nonviral therapeutic targets. Large-scale RNA interference (RNAi)-based screens have identified nearly a thousand candidate host factors, but there is little agreement among studies and few factors have been validated. Here we demonstrate that a genome-wide CRISPR-based screen identifies host factors in a physiologically relevant cell system. We identify five factors, including the HIV co-receptors CD4 and CCR5, that are required for HIV infection yet are dispensable for cellular proliferation and viability. Tyrosylprotein sulfotransferase 2 (TPST2) and solute carrier family 35 member B2 (SLC35B2) function in a common pathway to sulfate CCR5 on extracellular tyrosine residues, facilitating CCR5 recognition by the HIV envelope. Activated leukocyte cell adhesion molecule (ALCAM) mediates cell aggregation, which is required for cell-to-cell HIV transmission. We validated these pathways in primary human CD4⁺ T cells through Cas9-mediated knockout and antibody blockade. Our findings indicate that HIV infection and replication rely on a limited set of host-dispensable genes and suggest that these pathways can be studied for therapeutic intervention.

Viruses are obligate intracellular pathogens that, owing to their small genomes and a limited number of encoded proteins, exploit host proteins for entry, replication, and transmission. Identification of such host proteins, also termed host dependency factors (HDFs), is particularly important for identifying therapeutic targets. This strategy is especially useful for pathogens that undergo rapid mutation, because therapeutic targeting of host rather than viral proteins is associated with a much higher barrier to drug resistance[1].

HDFs that are dispensable for cellular viability yet are critical for productive infection may be ideal targets for therapeutic intervention. The discovery of CCR5 as a co-receptor for HIV infection of CD4⁺ T cells and macrophages led to the development of small-molecule inhibitors of CCR5 as therapeutic interventions[2] that are effective even following failure of virus-targeted therapy[3]. HDFs also present attractive targets for curative gene therapy, as is currently being developed for *CCR5* (ref. 4). The goal of this strategy is to engineer HIV resistance into CD4⁺ T cells of infected individuals through inactivation of *CCR5* via genomic editing. The only recorded case of an HIV cure occurred after a patient received a hematopoietic stem cell transplant from a donor who was homozygous for the inactivating CCR5Δ32 allele[5]. Individuals with this allelic variant, however, have increased susceptibility to some viral infections[6], cancers[7,8], and other diseases[9], suggesting that gene therapy approaches will benefit from the identification of other non-essential host genes that are required for HIV infection.

Large-scale, RNAi-based screens have suggested 842 putative HIV HDFs[10–12], but most of these candidate genes scored in only one of the three screens (37 genes scored in more than one screen; 3 genes scored in all three studies), suggesting a high false-positive rate, low reproducibility, or both. RNAi-based screens have been improved by

[1]Ragon Institute of Massachusetts General Hospital (MGH), Massachusetts Institute of Technology (MIT), and Harvard University, Cambridge, Massachusetts, USA. [2]Harvard–MIT Health Sciences and Technology, Harvard Medical School, Boston, Massachusetts, USA. [3]Broad Institute of MIT and Harvard University, Cambridge, Massachusetts, USA. [4]Department of Biology, Massachusetts Institute of Technology, Cambridge, Massachusetts, USA. [5]Whitehead Institute for Biomedical Research, Cambridge, Massachusetts, USA. [6]David H. Koch Institute for Integrative Cancer Research at MIT, Cambridge, Massachusetts, USA. [7]Department of Cellular and Molecular Pharmacology, California Institute for Quantitative Biosciences, QB3, University of California at San Francisco (UCSF), San Francisco, California, USA. [8]Gladstone Institute of Virology and Immunology, J. David Gladstone Institutes, San Francisco, California, USA. [9]Biological Sciences in Public Health, Harvard T.H. Chan School of Public Health, Boston, Massachusetts, USA. [10]Howard Hughes Medical Institute, Massachusetts General Hospital and Harvard Medical School, Boston, Massachusetts, USA. [11]Department of Microbiology and Immunology, University of California at San Francisco, San Francisco, California, USA. [12]Diabetes Center, University of California at San Francisco, San Francisco, California, USA. [13]Department of Medicine, University of California at San Francisco, San Francisco, California, USA. [14]Innovative Genomics Initiative (IGI), University of California, Berkeley, Berkeley, California, USA. [15]UCSF Helen Diller Family Comprehensive Cancer Center, University of California at San Francisco, San Francisco, California, USA. [16]Howard Hughes Medical Institute, Department of Biology, Massachusetts Institute of Technology, Cambridge, Massachusetts, USA. [17]Department of Systems Biology, Harvard Medical School, Boston, Massachusetts, USA. [18]Massachusetts General Hospital Cancer Center, Boston, Massachusetts, USA. [19]Institute of Medical Engineering and Sciences, Massachusetts Institute of Technology, Cambridge, Massachusetts, USA. [20]These authors contributed equally to this work. Correspondence should be addressed to D.M.S. (sabatini@wi.mit.edu), E.S.L. (lander@broadinstitute.org), N.H. (nhacohen@mgh.harvard.edu) or B.D.W. (bwalker@mgh.harvard.edu).

Received 30 June; accepted 15 November; published online 19 December 2016; doi:10.1038/ng.3741

the generation of high-coverage short hairpin RNA (shRNA) libraries, with up to 30 shRNAs targeting each gene[13], and analytical methods such as ATARiS and RIGER[14,15], but issues of sensitivity and specificity remain. Moreover, because the screens were performed in non-physiologically relevant cells, it is unclear whether these candidate HDFs are necessary for HIV infection in primary CD4$^+$ T cells and whether their loss affects normal cellular viability.

It has been demonstrated that a CRISPR–Cas9-based genetic screening approach using lentiviral single-guide RNA (sgRNA) libraries can enable pooled loss-of-function screens with greater sensitivity and specificity than RNAi-based screens and that the technology can identify cell-essential genes and mediators of drug resistance[16–19].

We conducted a CRISPR-based genetic screen in a naturally susceptible T cell line using a high-complexity, genome-wide sgRNA library. We identified five host genes that, when inactivated, conferred robust protection from HIV infection. These included genes encoding the canonical HIV co-receptors CD4 (*CD4*) and CCR5 (*CCR5*), and three encoding factors not identified in previous screens (*TPST2*, *SLC35B2*, and *ALCAM*). Loss of these factors did not impair cell viability, suggesting that they may represent attractive targets for therapeutic intervention. Finally, we developed a CRISPR-based approach to validate host factors for CCR5-tropic HIV strains in primary human CD4$^+$ T cells and demonstrated the importance of the cellular pathways identified by our screen in mediating efficient HIV infection. Our approach thus allows for highly specific, unbiased identification of host dependencies in physiologically relevant host cells and can be generalized to other epidemic and pandemic viruses.

RESULTS

A genome-wide CRISPR screen for HIV host dependency factors

To identify host genes that are important in facilitating HIV infection, we first engineered a physiologically relevant CD4$^+$ T cell line model suitable for pooled CRISPR-based screening, which we named 'GXRCas9' (**Fig. 1a**,**b** and **Supplementary Note**). Productive HIV infection of these cells leads to expression of GFP, thereby allowing the cellular infection state to be monitored at the single-cell level by flow cytometry. We selected the CCR5-tropic HIV-1 strain JR-CSF for our screen, as almost all known transmitted founder strains of HIV-1, which establish *de novo* infection in naive hosts, are CCR5-tropic[20].

We performed a pooled genome-wide screen using a lentiviral library containing 187,536 sgRNAs targeting 18,543 protein-coding human genes (average of 10 sgRNAs/gene) and 1,504 nontargeting control sgRNAs (those that do not target protein-coding sequences) (**Supplementary Table 1**). We infected 200 million GXRCas9 cells (~1,000 cells/sgRNA) with the library and selected the sgRNA-expressing cells with puromycin. One week after sgRNA library infection, we spin-infected 200 million cells with JR-CSF at a multiplicity of infection (MOI) of 0.025. A GFP$^+$ population (~10–20%; data not shown) was readily detectable 1 week after infection. After two additional weeks, we re-infected the cells with JR-CSF and cultured them for an additional 10 d, but now we found no change in viability or reporter-driven GFP expression, suggesting that the remaining cells harbored genetic knockouts that rendered them resistant to HIV infection. In contrast to the parental cell line, the majority of the surviving mutants lacked either CD4 or CCR5 (**Fig. 1c**). A subpopulation of the surviving cells retained high expression of CD4 and CCR5 on the cell surface, suggesting that our screen identified additional host factors for HIV infection (**Fig. 1c**).

Next we isolated viable, GFP$^-$ cells by FACS and used massively parallel sequencing to measure the abundance of all sgRNAs from this population, an initial population of cells collected prior to HIV infection, and a population of cells propagated for 6 weeks without HIV infection. For each gene, we calculated its score as the $\log_2$-transformed fold change in the abundance of the fifth highest-scoring sgRNA (**Supplementary Table 2**). Five genes scored strongly above background levels: *CD4*, *CCR5*, and three additional genes (*TPST2*, *SLC35B2*, and *ALCAM*) (**Fig. 1d**). For each gene, at least five and up to ten sgRNAs were enriched, whereas nearly all of the sgRNAs targeting *CXCR4* (which encodes an HIV co-receptor that is not used by JR-CSF) or a control gene, the GTPase-encoding *RAP2A*, did not score (**Fig. 1e**). The same five genes were identified by calculating the gene score as the mean of the individual $\log_2$-transformed fold change values in the abundance of each of the sgRNAs targeting a given gene (**Supplementary Fig. 1**).

Validation of TPST2 and SLC35B2 as host dependency factors

To understand how loss of *TPST2* and *SLC35B2* confers protection against HIV infection, we used the CRISPR–Cas9 system to generate clonal GXRCas9 cell lines null for the genes, as assessed by massively parallel sequencing of the predicted target sites and by qRT–PCR (**Supplementary Fig. 2**). Under normal culture conditions, *TPST2*-null and *SLC35B2*-null cells were viable and proliferated at rates comparable to those of wild-type cells and of knockout cells that were complemented with an sgRNA-resistant cDNA (**Fig. 2a**).

Consistent with the screen results, *TPST2*-null and *SLC35B2*-null cells showed robust resistance to infection with JR-CSF (MOI = 1), similar to that observed in *CCR5*-null cells. Re-expression of an sgRNA-resistant cDNA encoding the missing gene completely ablated this resistance, whereas no changes in HIV susceptibility were seen after transduction with an irrelevant control gene, *RAP2A* (**Fig. 2b**). *TPST2*-null and *SLC35B2*-null cells appeared healthy following HIV challenge, whereas cells that were transduced with a nontargeting sgRNA appeared grossly apoptotic (**Fig. 2c**). To extend the physiological relevance, we also infected these cell lines with Rejo.c, a CCR5-tropic transmitted founder HIV-1 strain[21], and obtained similar results (**Fig. 2b**).

Host proteins that are hijacked by pathogens once inside the cell are often used for essential cellular functions such as transcription and translation[22,23], whereas host factors used for pathogen entry are often dispensable for cell viability, as is the case for CCR5 and CXCR4 (canonical co-receptors for HIV entry) and for CD55 (a glycoprotein recently found to be essential for malaria entry into erythrocytes)[24]. Given the normal proliferative capacity of the knockout cell lines, we investigated whether loss of *TPST2* or *SLC35B2* confers protection against HIV entry by using a previously reported β-lactamase-based viral fusion assay to specifically detect fusion of HIV virions to a target cell[25] (**Fig. 2d** and Online Methods). We found that loss of either *TPST2* or *SLC35B2* protected cells from viral entry, and that susceptibility was restored upon add-back of the inactivated gene (**Fig. 2e**).

CCR5 sulfation is critical for HIV entry

We sought to determine the mechanisms by which TPST2 and SLC35B2 facilitate viral entry. SLC35B2 transports the activated sulfate donor, 3′-phosphoadenosine-5′-phosphosulfate (PAPS), from the cytosol, where it is synthesized, into the lumen of the Golgi apparatus, where it is used by a variety of enzymes to decorate sugars and proteins[26]. One such *trans*-Golgi-resident enzyme, TPST2, catalyzes the *O*-sulfation of tyrosines on secretory and plasma membrane proteins[27].

We tested the importance of cellular sulfation for HIV entry by culturing GXRCas9 cells in medium that was depleted of sulfates and in the presence of sodium chlorate, an inhibitor of sulfation[28]. Using the β-lactamase-based viral fusion assay, we found that sulfate-depleted

© 2017 Nature America, Inc., part of Springer Nature. All rights reserved.

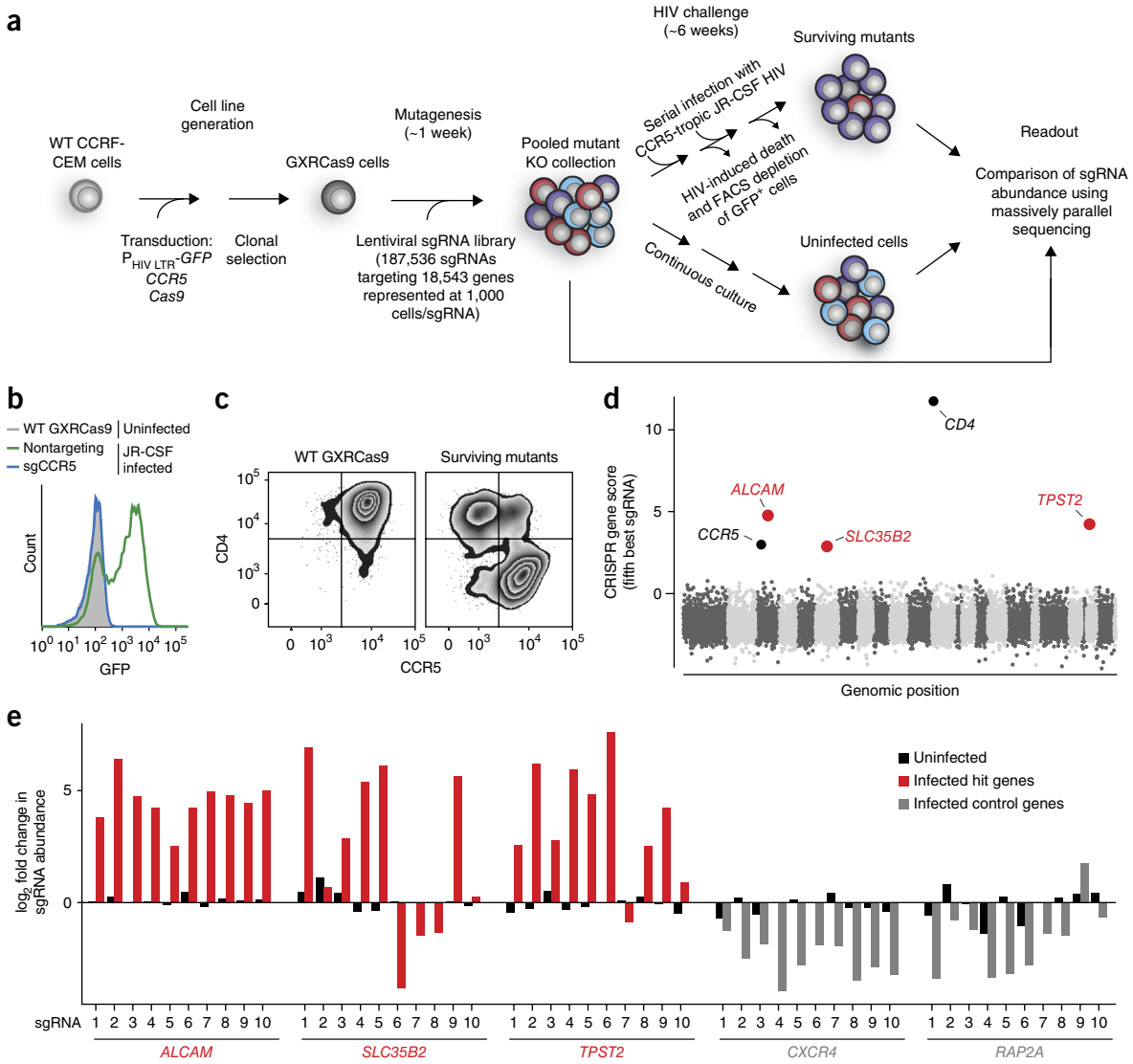


Figure 1 A pooled, genome-wide CRISPR screen for HIV HDFs. (**a**) Outline of the genome-wide CRISPR screen strategy. WT, wild type; KO, knockout. (**b**) Flow cytometry analysis (representative of five independent experiments) of cells infected with the HIV-1 strain JR-CSF and expressing GFP as a reporter of productive HIV infection. Where indicated, cells were transduced with sgCCR5 or an sgRNA that does not target protein-coding sequences in the human genome (nontargeting control). (**c**) Flow cytometry analysis (representative of three independent experiments) quantifying CD4 and CCR5 expression on the surface of wild-type GXRCas9 cells and GXRCas9 cells that were transduced with the genome-wide sgRNA library and serially infected with HIV-1 strain JR-CSF. (**d**) Log_2-transformed fold change in the abundance of the fifth most enriched sgRNA for every gene following HIV infection. See also **Supplementary Figure 1** and **Supplementary Table 1**. (**e**) Enrichment of individual sgRNAs for three candidate HDFs and two control genes. Values indicate log_2-transformed fold change in abundance following HIV infection. Values for the uninfected group are from GXRCas9 cells that were transduced with the genome-wide sgRNA library and cultured for 3 weeks.

cells are protected from viral fusion relative to cells cultured under standard conditions (**Fig. 3a**). This effect was not due to a loss of heparan sulfate proteoglycans, an important class of cell surface proteins that are synthesized in an SLC35B2-dependent manner and that are known to mediate cell surface attachment of various pathogens including *Chlamydia trachomatis*[29,30], as pretreatment of the cells with heparinase did not affect viral entry in our assay (**Fig. 3a**).

Previous studies have demonstrated that tyrosine sulfation at the N terminus of CCR5 facilitates interactions with HIV gp120 (ref. 31). Because TPST2 sulfates CCR5 on these tyrosine residues[32], we hypothesized that loss of SLC35B2 protects against HIV infection by depriving TPST2 of PAPS (**Fig. 3b**). To investigate this possibility, we assessed CCR5 surface expression by flow cytometry using sulfation-sensitive and sulfation-insensitive CCR5-specific antibodies[33]. Consistent with our hypothesis, nearly all surface CCR5 was sulfated in wild-type GXRCas9 cells, whereas none was sulfated in *TPST2*-null and *SLC35B2*-null cells. The total levels of CCR5 on the surface of these cells were unchanged, and add-back of the relevant gene rescued CCR5 sulfation (**Fig. 3c**).

ALCAM–ALCAM interactions mediate GXRCas9 cell aggregation

To validate *ALCAM*, we transduced GXRCas9 cells with an sgRNA targeting *ALCAM* and isolated *ALCAM*-null cells by FACS; we re-expressed an sgRNA-resistant *ALCAM* cDNA in these cells by retroviral transduction (**Fig. 4a**). Loss of *ALCAM* did not compromise cell proliferation (**Fig. 4b**). Unexpectedly, *ALCAM*-null cells showed

© 2017 Nature America, Inc., part of Springer Nature. All rights reserved.

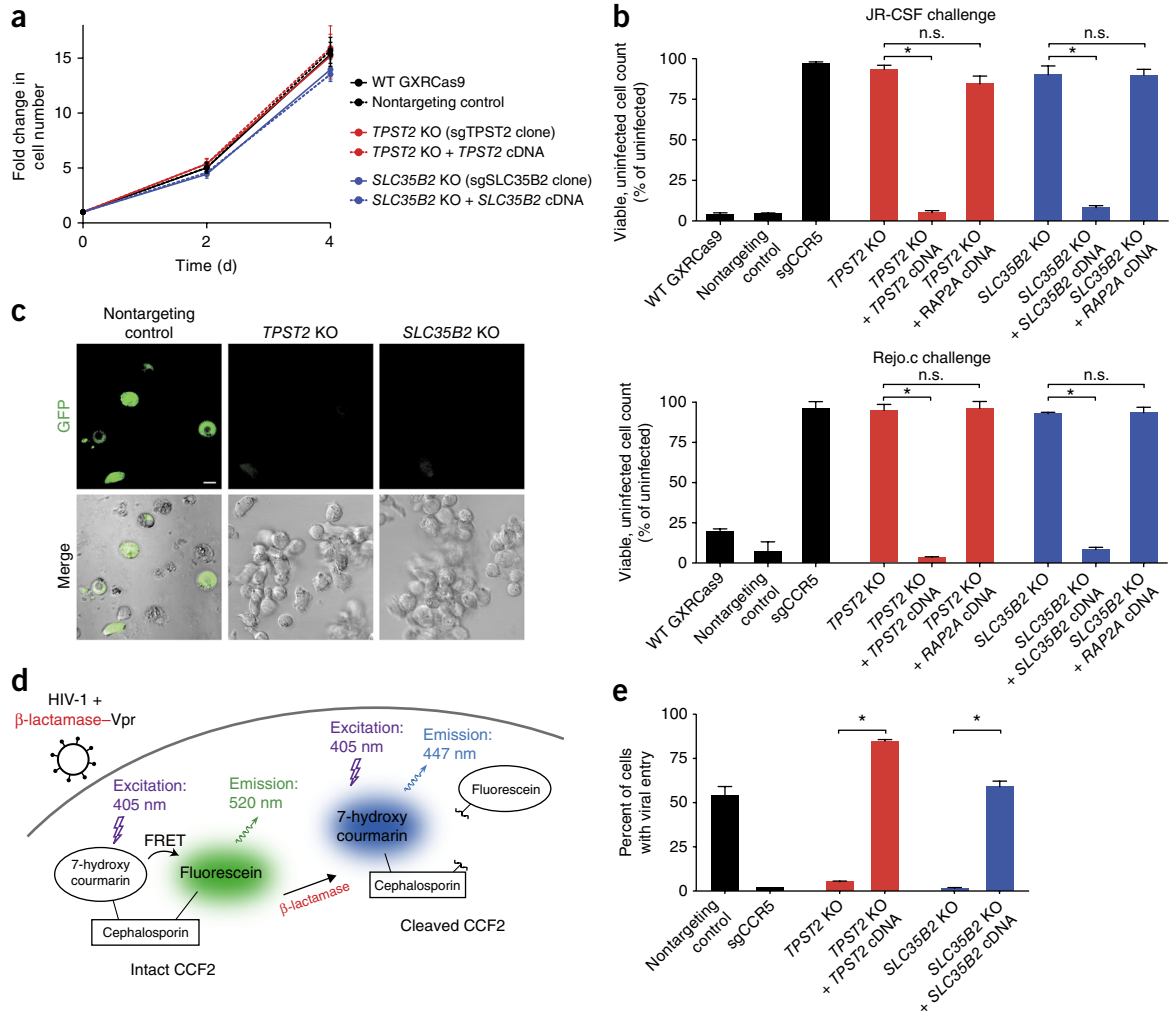


Figure 2 Loss of *TPST2* or *SLC35B2* confers strong protection against HIV infection and entry without compromising host cell viability. (**a**) Cell proliferation assays for wild-type cells, *TPST2*-knockout and *SLC35B2*-knockout GXRCas9 cells, nontargeting-sgRNA-transduced cells, and cells with rescued *TPST2* and *SLC35B2* expression. Error bars, s.d. from six replicate wells. (**b**) Virus challenge assays with JR-CSF (top) and Rejo.c, a patient-derived transmitted founder strain of HIV (bottom). Three days following HIV infection (MOI = 1), viable, GFP$^-$ cells were counted and their numbers were normalized to those under a mock-infected condition. Error bars, s.d. from triplicate wells. $^*P < 0.01$; n.s., not significant; by Welch's *t* test. Individual *P* values are as follows. JR-CSF: *TPST2*, $^*P < 0.0001$; n.s., $P = 0.0637$; *SLC35B2*, $^*P = 0.0009$; n.s., $P = 0.9714$; Rejo.c: *TPST2*, $^*P = 0.0005$; n.s., $P = 0.6478$; *SLC35B2*, $^*P < 0.0001$; n.s., $P = 0.7751$. (**c**) Confocal microscopy images (representative of six images acquired per condition) of GXRCas9 cells transfected with a nontargeting control sgRNA (left) and of *TPST2*-null (middle) and *SLC35B2*-null (right) GXRCas9 cells following HIV challenge. GFP is a reporter for productive HIV infection. Bottom, merged images from the differential interference contrast (DIC) and GFP channels. Scale bar, 5 µm. (**d**) Schematic of the HIV entry assay. β-lactamase–Vpr fusion protein is packaged in HIV virions. Target cells are loaded with CCF2, a FRET donor–acceptor pair linked by a β-lactam ring. Upon viral fusion, the virus-delivered β-lactamase cleaves off the intracellular FRET acceptor, leading to a shift in the emission wavelength. (**e**) HIV entry assays for *TPST2*-null and *SLC35B2*-null GXRCas9 cells, wild-type cells, nontargeting-control-sgRNA-transduced cells, and cells with rescued *TPST2* and *SLC35B2* expression. Error bars, s.d. from triplicate wells. $^*P < 0.01$ by Welch's *t* test. $^*P < 0.0001$ for *TPST2*; $^*P = 0.0001$ for *SLC35B2*.

no protection against JR-CSF infection (MOI = 1) (**Fig. 4c**), despite the fact that all ten sgRNAs targeting *ALCAM* in the library were enriched in the screen (**Fig. 1e**). We observed that *ALCAM*-null cells grew as single cells under standard culture conditions, whereas wild-type GXRCas9 cells, in a manner similar to activated primary CD4$^+$ T cells, formed aggregates (**Fig. 4d**). Re-expression of *ALCAM* rescued the aggregation phenotype.

The precise cellular function of ALCAM, a cell adhesion molecule expressed on activated T cells, monocytes, and dendritic cells[34], is not fully understood[35,36]. *In vitro* experiments have demonstrated that antibody blockade of ALCAM affects diapedesis of monocytes, but not T cells, in a model for the human blood–brain barrier[37]. Systemic anti-ALCAM administration has thus been proposed as a therapy for HIV-associated neurocognitive disorders. The interaction of ALCAM with CD6, a cell adhesion and signaling molecule found on the surface of T cells, is involved in stabilizing the immunological synapse between T cells and antigen-presenting cells[38]. However, homotypic ALCAM–ALCAM interactions have also been described[39].

To determine which of these potential interactions mediates the aggregation of GXRCas9 cells, we co-cultured *ALCAM*-null cells and wild-type cells labeled with distinct fluorescent dyes (**Fig. 4e**). Aggregates in co-culture were composed solely of wild-type cells, whereas *ALCAM*-null cells remained as singlets (**Fig. 4f**). Add-back of the *ALCAM* gene and co-culture with wild-type cells yielded mixed

© 2017 Nature America, Inc., part of Springer Nature. All rights reserved.

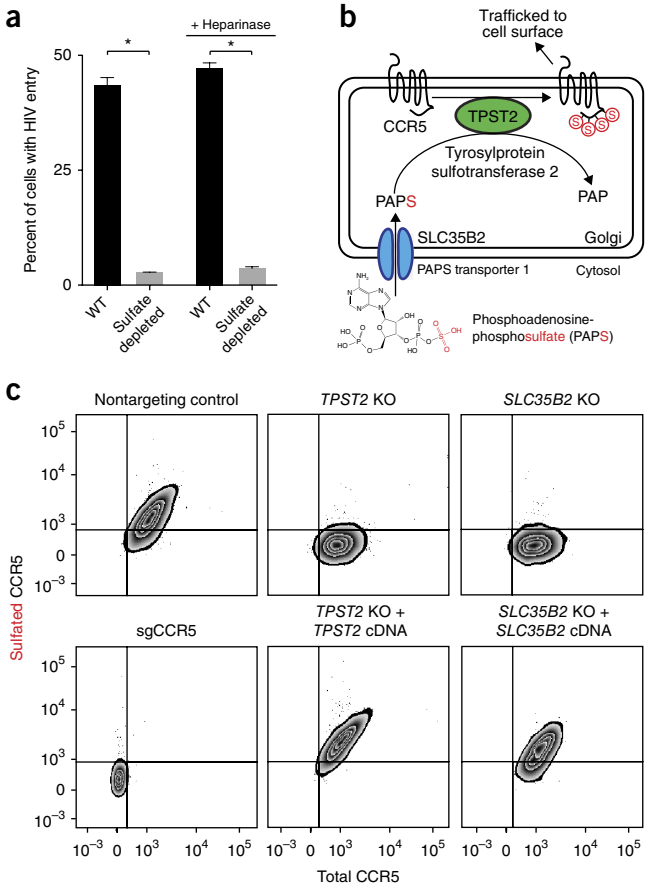


Figure 3 SLC35B2 and TPST2 function in a common pathway for the sulfation of CCR5. (**a**) HIV entry assays for GXRCas9 cells cultured in standard medium or in sulfate-free medium with sodium chlorate, an inhibitor of cellular sulfation. Where indicated, heparinase was used to remove cell surface heparan sulfates. Error bars, s.d. from triplicate wells; $*P < 0.01$ by Welch's t test. $*P = 0.0005$ for no heparinase; $*P < 0.0001$ for heparinase. (**b**) Schematic of SLC35B2 and TPST2 sulfating CCR5 within the Golgi apparatus. (**c**) Flow cytometry analysis (representative of two independent experiments) quantifying total and sulfated CCR5 expression on the cell surface of GXRCas9 cells with a nontargeting control sgRNA, *CCR5*-null GXRCas9 cells, and cells with ablated or rescued *TPST2* and *SLC35B2* expression.

aggregates. Confocal microscopy analysis of GXRCas9 cells that were stained with an ALCAM-specific antibody showed strong polarization of ALCAM to the site of cell–cell contacts (**Fig. 4g**), supporting a role for ALCAM in contact mediation. Taken together, these data demonstrate that homotypic interactions between ALCAM molecules on opposing cells are required for GXRCas9 cell aggregation.

Loss of ALCAM disrupts cell-to-cell HIV transmission

Because of the loss of cell-to-cell aggregation observed in *ALCAM*-null cells, we hypothesized that loss of ALCAM interrupts cell-to-cell transmission, thereby attenuating infection. This model reconciles the results from the primary screen, which used a low virus dose (MOI = 0.025) over 6 weeks, with those from the short-term validation assay, which used an MOI of 1 and would not require cell-to-cell transmission for widespread HIV infection. Consistent with this, *ALCAM*-null cells showed dramatic protection in viral challenge assays performed at a low MOI over a longer period (**Supplementary Fig. 3**). To confirm that the protective effect was due to inhibition of cell-to-cell transmission, we co-cultured HIV-infected wild-type 'donor' cells with uninfected, fluorescently labeled *ALCAM*-null 'acceptor' cells and assessed the degree of infection of the labeled cells after 4 d (**Fig. 5a**). *ALCAM*-null cells were completely protected from infection, whereas cells that were transduced with a nontargeting control showed substantial infection and death (**Fig. 5b**). *ALCAM* add-back ablated this protection, whereas add-back of a control gene, *RAP2A*, had no effect.

To demonstrate that our assay isolated the effects of cell-to-cell transmission, we placed the infected wild-type cells in a 0.45-μm pore Transwell insert, which permits passage of free HIV virions but not cells. In this setting, we found that the cells were protected from HIV infection irrespective of *ALCAM* genotype, confirming the necessity of cell-to-cell contacts for infection (**Fig. 5b**).

We assessed the degree of cell-to-cell HIV transmission when one, both, or neither of the donor and acceptor cell lines lacked ALCAM. Consistent with the model that homotypic ALCAM interactions mediate cell aggregation and, therefore, cell-to-cell transmission, infection of the acceptor cells was only observed when both the donor and acceptor cells were ALCAM$^+$ (**Fig. 5c**).

We investigated whether protection against cell-to-cell HIV transmission was a direct result of disrupting cell aggregation or whether cell-to-cell contacts mediated by ALCAM promoted HIV infection specifically. We labeled the surface of cells with complementary oligonucleotides[40] to cause aggregation of *ALCAM*-null cells in an ALCAM-independent manner (**Fig. 5d**). Cells labeled with complementary oligonucleotides formed aggregates that seemed similar to those seen in wild-type GXRCas9 cells (**Fig. 5e**). Using these cells in the cell-to-cell transmission assay, we found that this nonspecific aggregation of *ALCAM*-null cells fully abrogated protection against cell-to-cell transmission (**Fig. 5f**). By contrast, *ALCAM*-null cells that were labeled with identical (i.e., noncomplementary) oligonucleotides were protected in a manner similar to that seen in previous assays in which there was no oligonucleotide labeling.

Taken together, these data indicate that loss of ALCAM confers strong protection against cell-to-cell HIV transmission by disrupting cell aggregation and that restoring aggregation by other means restores cell-to-cell transmission.

CRISPR–Cas9-mediated genome editing in primary CD4$^+$ T cells

Next, to establish the physiological relevance of our primary screen results, we developed an assay to validate HDFs for infection by CCR5-tropic HIV in primary CD4$^+$ T cells using CRISPR–Cas9. Primary peripheral CD4$^+$ T cells isolated from the blood of healthy donors were activated by using antibodies to CD3 and CD28. Cells were then electroporated with ribonucleoprotein complexes (Cas9–RNPs), which consisted of the Cas9 nuclease bound to a gene-specific CRISPR RNA (crRNA) and the *trans*-activating crRNA (tracRNA)[41] (**Fig. 6a**). After 6 d in culture to allow for depletion of the targeted gene product, the cells were reactivated for 3 d to promote productive infection by a CCR5-tropic HIV strain.

Validation of SLC35B2 as an HDF in primary CD4$^+$ T cells

We targeted *SLC35B2* in primary CD4$^+$ T cells and assessed the sulfation state of cell-surface-expressed CCR5. Consistent with the results from GXRCas9 cells, we found that the majority of CCR5 was desulfated 9 d after transfection, whereas total CCR5 expression was unaffected (**Fig. 6b**). Cell-surface-expressed CCR5 was completely sulfated in cells transfected with the nontargeting control, as expected.

Taking advantage of the fact that gene editing does not occur in every cell following Cas9–RNP electroporation, we next challenged

© 2017 Nature America, Inc., part of Springer Nature. All rights reserved.

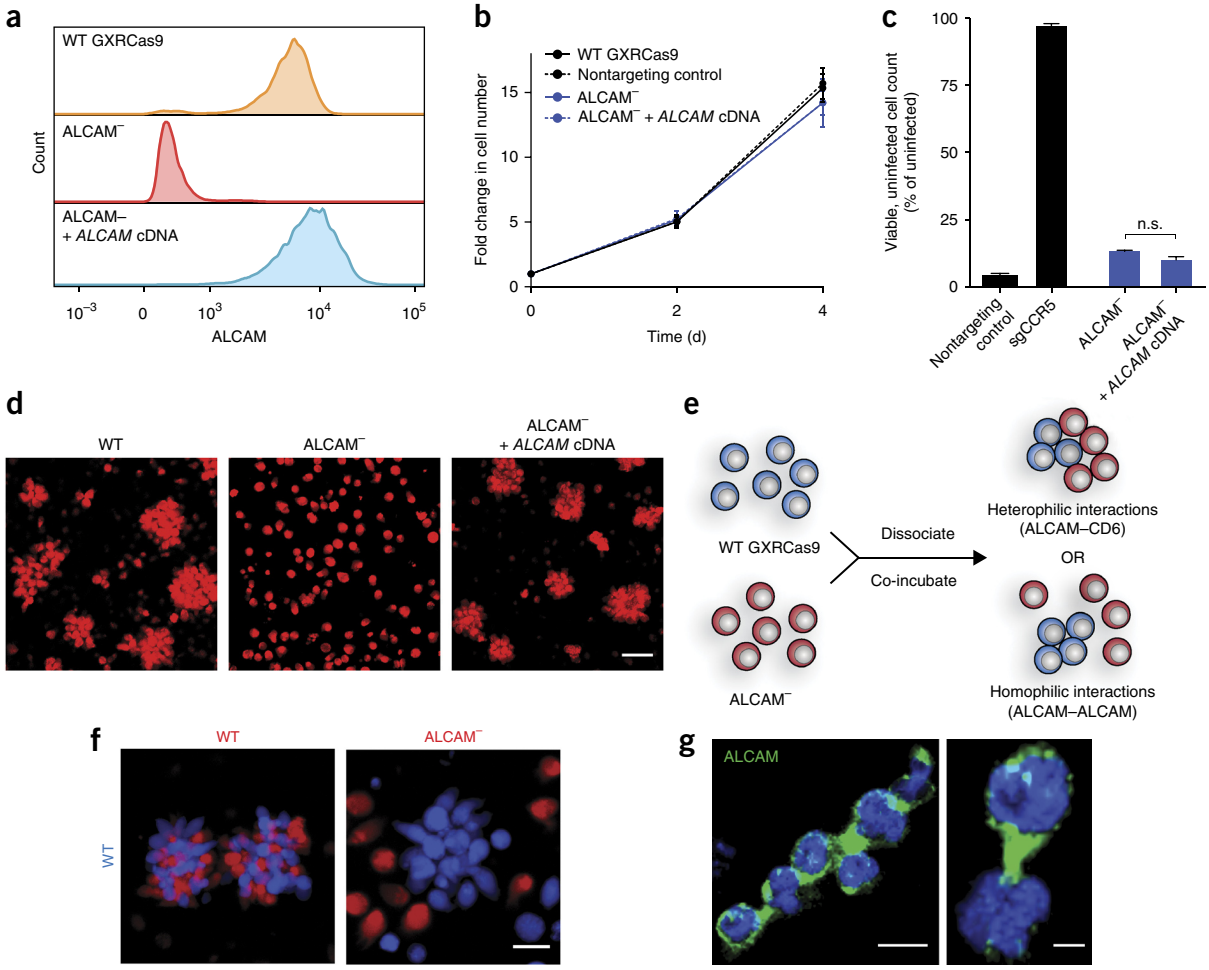


Figure 4 Homophilic ALCAM interactions are necessary for GXRCas9 cell aggregation. (**a**) Flow cytometry analysis (representative of four independent experiments) quantifying ALCAM expression on the cell surface of wild-type GXRCas9 cells and cells with ablated or rescued *ALCAM* expression. (**b**) Cell proliferation assays of wild-type GXRCas9 cells, cells transduced with a nontargeting control sgRNA, *ALCAM*-null cells, and *ALCAM*-rescued cells. Error bars, s.d. from six replicate wells. (**c**) Virus challenge assays with JR-CSF demonstrating that *ALCAM*-null cells lack protection against HIV infection at an MOI of 1. Error bars, s.d. from triplicate wells. n.s., $P = 0.0308$; by Welch's t test. (**d**) Confocal microscopy images (representative of five images acquired per condition) depicting the cellular aggregation phenotype of GXRCas9 cells with wild-type (left), null (middle), or rescued (right) *ALCAM* expression. Scale bar, 50 μm. (**e**) Schematic of the co-culture assay to distinguish between two models for ALCAM-mediated cell aggregation and their possible outcomes. Mixed aggregates will result from the co-culture of wild-type and *ALCAM*-null cells if aggregates are due to heterophilic ALCAM–CD6 interactions, whereas aggregates with only wild-type cells will result if aggregates are due to homophilic ALCAM–ALCAM interactions. (**f**) Confocal microscopy images (representative of ten images acquired per condition) demonstrating that *ALCAM*-null cells are not contained within aggregates. Scale bar, 20 μm. (**g**) Confocal microscopy images (representative of five images acquired per condition) of aggregates from wild-type GXRCas9 cells showing ALCAM (green) and DAPI (blue) staining. Scale bars, 10 μm (left) and 3 μm (right).

© 2017 Nature America, Inc., part of Springer Nature. All rights reserved.

these cells with HIV and assessed mutant allele frequency. In two donors, nearly all of the alleles in cells that survived either JR-CSF or Rejo.c challenge were mutated (**Fig. 6c**). To demonstrate that desulfation of CCR5 correlates with protection against HIV infection, we assessed the extent of CCR5 sulfation in HIV-challenged cells and found that cell-surface-expressed CCR5 on productively infected cells was exclusively sulfated (**Supplementary Fig. 4**). Correspondingly, CCR5 was desulfated on cells that remained uninfected following HIV challenge as compared to that in mock-challenged cells.

In a parallel approach, we assessed infection levels of edited primary CD4$^+$ T cells from two additional donors by intracellular flow staining for HIV gag (p24). We found that targeting either *CCR5* or *SLC35B2* conferred similar, high levels of protection as infection by JR-CSF but conferred no protection against infection by VSV-G-pseudotyped HIV (**Fig. 6d**), which infects cells in a CD4- and CCR5-independent manner. This selective protection is consistent with the model for *SLC35B2* presented (**Fig. 3b**).

Disrupting primary T cell aggregation hinders HIV spread

Having observed that *ALCAM* knockout yielded protection against cell-to-cell HIV transmission by disruption of GXRCas9 cell aggregation, we sought to recapitulate this protection in primary CD4$^+$ T cells, which aggregate after activation. Because activated primary CD4$^+$ T cells express lower (~10-fold lower) levels of *ALCAM* as compared to those in GXRCas9 cells (**Supplementary Fig. 5** and **Supplementary Table 3**), we looked for other molecules known to be involved in the aggregation of activated primary CD4$^+$ T cells, the most well-characterized of which are members of the intercellular adhesion molecule (ICAM) and lymphocyte function-associated

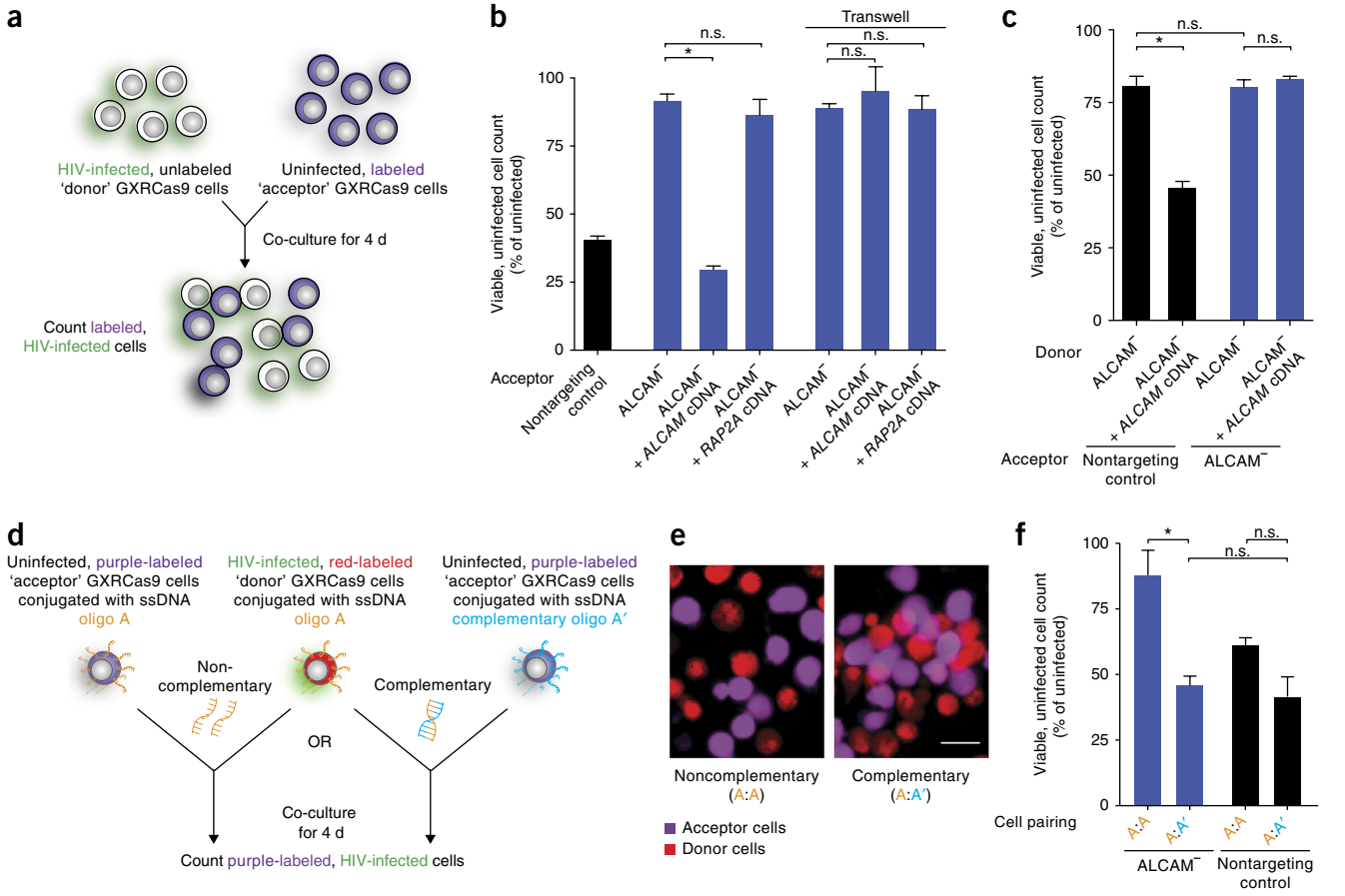


Figure 5 Loss of ALCAM protects against cell-to-cell transmission of HIV through disruption of cell aggregation. (**a**) Schematic of the cell-to-cell HIV transmission assay. Acceptor cells are fluorescently labeled and co-cultured with unlabeled, infected wild-type donor cells. After 4 d, the number of labeled, GFP⁻ viable cells is assessed by flow cytometry and cell counting and normalized to cell number under a matching condition in which donor cells were not infected. (**b**) Quantification of cell-to-cell transmission for wild-type donor cells and the acceptor cells indicated on the *x* axis. Where indicated, a 0.45-µm pore size Transwell was used to separate donor and acceptor cells for the entirety of the 4-d co-culture. Error bars, s.d. from triplicate wells. $*P < 0.0001$; n.s., not significant (without Transwell: n.s., $P = 0.2605$; with Transwell, n.s., $P = 0.3481$ (ALCAM⁻ versus ALCAM⁻ + *ALCAM* cDNA); n.s., $P = 0.8903$ (ALCAM⁻ versus ALCAM⁻ + *RAP2A* cDNA)); by Welch's *t* test. (**c**) Quantification of cell-to-cell transmission for the donor cells and acceptor cells indicated. Donor cells were either null or rescued for ALCAM expression, and acceptor cells were either wild type (nontargeting control) or null for ALCAM expression, as indicated. Error bars, s.d. from triplicate wells. $*P = 0.0002$; n.s., not significant (n.s., $P = 0.8425$ (ALCAM⁻ donor with ALCAM⁺ acceptor versus ALCAM⁻ donor with ALCAM⁻ acceptor); n.s., $P = 0.1959$ (ALCAM⁻ donor with ALCAM⁻ acceptor versus ALCAM⁻ donor expressing *ALCAM* cDNA with ALCAM⁻ acceptor)); by Welch's *t* test. (**d**) Schematic for ALCAM-independent cellular aggregation. As with the cell-to-cell HIV transmission assay, donor cells are infected and co-cultured with labeled acceptor cells. Donor and acceptor cells are both null for ALCAM expression and are labeled either with complementary oligonucleotides (A and A′) to induce aggregation or with identical oligonucleotides (A and A) as a control. ssDNA, single-stranded DNA. (**e**) Confocal microscopy images (representative of ten images acquired per condition) of oligonucleotide-conjugated cells. Scale bar, 20 µm. (**f**) Quantification of cell-to-cell transmission among *ALCAM*-null cells labeled with complementary or noncomplementary oligonucleotides. Error bars, s.d. from triplicate wells. $*P = 0.0092$; n.s., not significant (n.s., $P = 0.4479$ (ALCAM⁻ cells with complementary oligonucleotides versus ALCAM⁺ cells with complementary oligonucleotides); n.s., $P = 0.0334$ (ALCAM⁺ cells with noncomplementary versus complementary oligonucleotides)); by Welch's *t* test.

antigen (LFA) families[42,43]. A recent study found that T cells isolated from *Icam1*-null mice failed to aggregate after activation[44], analogous to the phenotype observed after *ALCAM* knockout in GXRCas9 cells. We observed that GXRCas9 cells express very low levels of *ITGAL*, which encodes CD11a, one of two subunits of LFA-1 (**Supplementary Fig. 5** and **Supplementary Table 3**).

We therefore investigated the effect of disrupting ICAM–LFA-1 interactions on cell-to-cell HIV transmission in primary CD4⁺ T cells. Using the Cas9–RNP gene editing approach, we generated a population of *ITGAL*-null primary CD4⁺ T cells (**Fig. 6a**). We then co-cultured productively infected 'donor' cells with uninfected, fluorescently labeled 'acceptor' cells and found that knockout of *ITGAL* in both donor and acceptor cells attenuated cell-to-cell transmission as compared to that observed in wild-type donor and acceptor cells (**Fig. 6e**). Consistent with the heterophilic nature of the ICAM–LFA-1 interaction, knockout of *ITGAL* in only the donors did not confer protection (**Supplementary Fig. 6a**). Similar protection against cell-to-cell HIV transmission was observed by using an antibody cocktail directed against ICAM-1 and LFA-1 but not with a control antibody directed against CD45, which is also highly expressed on the surface of T cells, suggesting that the protection was not due a nonspecific 'blocking' effect (**Supplementary Fig. 6b**,**c**).

DISCUSSION

Our CRISPR-based screen identified five HDFs that are required for productive HIV infection. In addition to genes encoding the canonical

© 2017 Nature America, Inc., part of Springer Nature. All rights reserved.

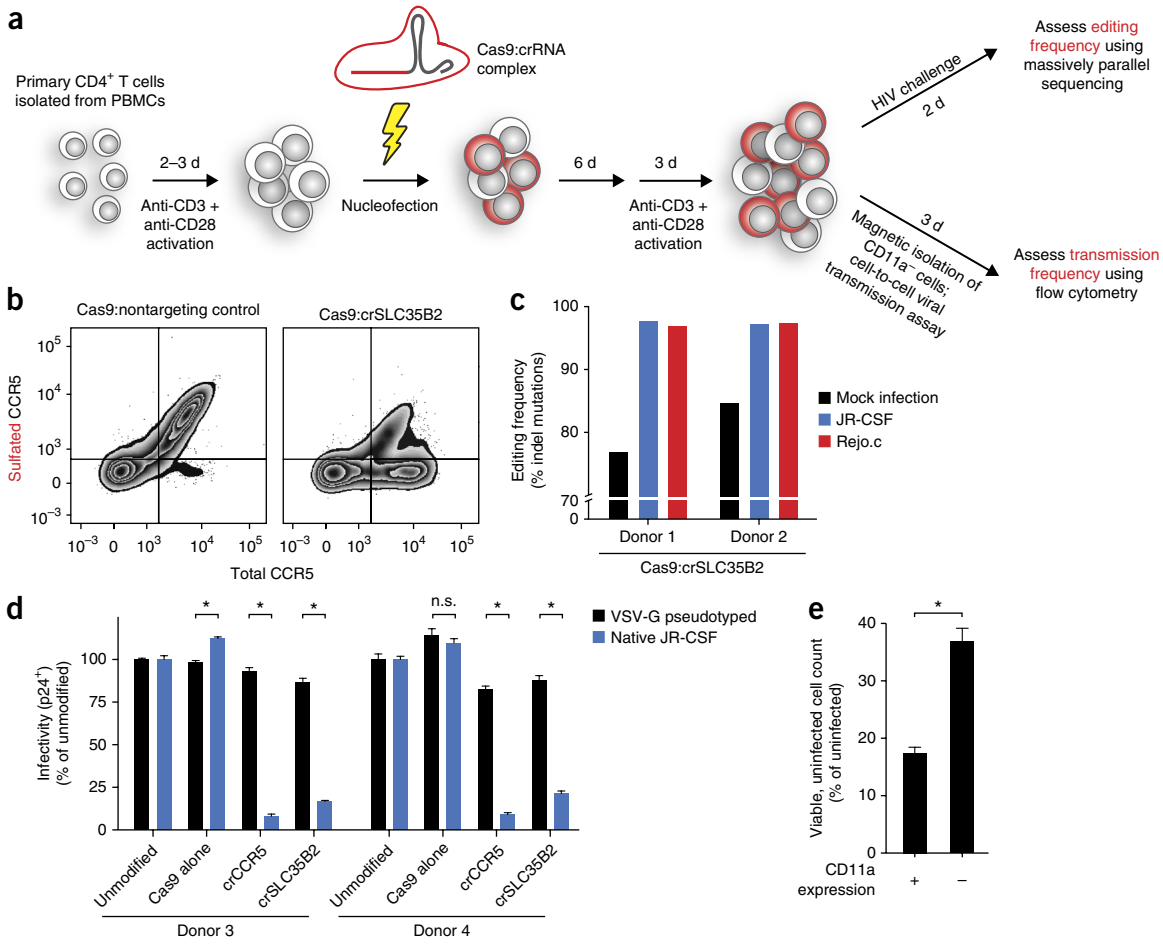


Figure 6 CRISPR-based approach for validation of HIV HDFs in primary human CD4+ T cells. (**a**) Schematic of the approach. Primary CD4+ T cells are activated using antibodies to CD3 and CD28 and nucleofected with Cas9–RNPs. After 6 d, cells are re-activated for 3 d and either challenged directly with HIV and sequenced at the sgRNA target site to assess mutation frequency or purified for CD11a− cells using magnetic beads and used in a cell-to-cell HIV transmission assay. PBMCs, peripheral blood mononuclear cells. (**b**) Representative flow cytometry analysis for the cell surface expression of total and sulfated CCR5 in primary CD4+ T cells that were transfected with the indicated Cas9–RNP complexes. Cells were analyzed at the time of HIV infection. (**c**) Indel mutation frequency in primary CD4+ T cells from two donors following challenge with JR-CSF or Rejo.c, as compared to that in a mock infection (also see **Supplementary Fig. 4**). (**d**) Flow cytometry analysis of intracellular HIV gag in Cas9–RNP-transfected primary CD4+ T cells from two additional donors. Values are normalized to those of untransfected cells for each respective virus type. Entry of VSV-G-pseudotyped HIV is independent of CD4 and CCR5. Error bars, s.d. from triplicate wells. *$P < 0.01$; n.s., not significant ($P = 0.1715$); by Welch's t test. *$P < 0.0001$ for all, except donor 3 crSLC35B2 ($P = 0.0002$). (**e**) Cell-to-cell HIV transmission assays in primary CD4+ T cells transfected with Cas9:crITGAL. The assay is set up as in **Figure 5**, except that donor cells were infected 24 h prior to co-culture and co-culture was for 2 d. Readout is by flow cytometry following intracellular staining for HIV gag. See **Supplementary Figure 6**. Error bars, s.d. from triplicate wells; *$P = 0.0036$ by Welch's t test.

HIV co-receptors CD4 and CCR5, we identified *TPST2*, *SLC35B2*, and *ALCAM*, none of which was among the hundreds of genes identified in previous RNAi-based screens[10–12]. We defined the mechanisms by which these genes facilitate HIV infection and validated these pathways in primary CD4+ T cells. Loss of TPST2, SLC35B2, or ALCAM did not affect cellular fitness. These results indicate that HIV relies on a limited number of non-essential host proteins for replication and suggest pathways for potential therapeutic intervention.

Some key methodological differences can probably explain the large discrepancy in the numbers of hits obtained in our screen as compared to those in the RNAi-based screens.

First, the studies use different methods to perturb gene function. Previous studies relied on RNAi-mediated knockdown, which only partially suppresses target gene expression levels and can have off-target effects on other mRNAs[45]. Additionally, the arrayed screen format limited the number of small interfering RNA (siRNA) reagents targeting each gene (many genes with only a single scoring siRNA were 'called' as candidate HDFs), increasing the likelihood of false-positive and false-negative results. These factors probably contributed to the low overlap observed between each data set. We were unable to detect any protection against JR-CSF infection in GXRCas9 cells that were transduced with an sgRNA targeting *RELA*, the single non-essential-gene hit that was identified in all three prior screens (**Supplementary Fig. 7**).

In contrast, we performed a pooled CRISPR–Cas9-based screen using a genome-wide sgRNA library that was optimized for high target cleavage activity. Here Cas9-mediated cleavage inactivates target genes at the DNA level, enabling the generation of null alleles. This approach shows minimal activity at secondary, off-target sites, most of which reside in noncoding regions. Furthermore, previous screens for cell-essential genes, which are more technically demanding (because cleavage of the target gene must occur in the majority of

© 2017 Nature America, Inc., part of Springer Nature. All rights reserved.

© 2017 Nature America, Inc., part of Springer Nature. All rights reserved.

cells carrying an sgRNA construct to reliably assess essentiality), have demonstrated that the effective coverage of our library is high[18].

Second, the RNAi screens were performed in different cell line models (derived from HEK-293 and HeLa cells), which were chosen to facilitate efficient siRNA transfection and high-throughput imaging but which are dissimilar in many respects to natural target cells for HIV infection. Although these cell line models have been frequently used to study HIV infection, they are not naturally susceptible to HIV infection. Therefore, to more faithfully model the physiological HIV infection process, we conducted our screen in a $CD4^+$ T cell leukemia line and confirmed our findings in primary $CD4^+$ T cells.

Third, the screen end points and the criteria for determining candidate genes also differed greatly. Genes from the RNAi-based screens were evaluated in an arrayed format 1–2 d after HIV infection, at which time weakly protective hits or those that delay, but do not suppress, the course of infection would be expected to score. In addition, because CRISPR predominantly generates null alleles, our screen was poised to detect genes that were dispensable for proliferation and viability. Mutants obtained in our screens survived serial challenge with replication-competent HIV for several weeks. This stringent selection process selected for genes whose loss conferred robust, sustained protection against HIV infection and did not also affect cell viability. We note that, whereas loss of these genes does not affect cell viability *in vitro*, perturbing their expression may have biological consequences at the organismal level. For example, *Tpst2*-deficient mice are viable but have thyroid hypoplasia[46]. Similarly, *Itgal*-deficient mice are viable and grossly normal but, as may be expected, have peripheral leukocytosis[47] and immune dysfunction[48]. Zebrafish lacking the homolog of *SLC35B2* have cartilage defects[49]. For the purposes of gene-editing-based therapies, some of these effects may be avoided by limiting gene editing to specific cell types (such as T cells or hematopoietic stem cells). However, further preclinical investigation will be needed to determine whether these genes may be suitable therapeutic targets.

Studies to map the HIV–human protein–protein interactome[50], as well as more targeted studies, have identified dozens of host genes with putative roles in facilitating or restricting HIV infection[1]. There are several reasons as to why our screen would not be expected to identify these genes. First, by requiring a high degree of protection, we would expect to identify only host factors that are necessary for productive HIV infection (**Supplementary Note**). Second, many host factors are likely to be essential; indeed, in contrast to *TPST2*, *SLC35B2*, and *ALCAM*, many known or candidate HIV HDFs are among the 10% highest-scoring genes reported in an essentiality screen[18] (**Supplementary Fig. 8**). Third, the genes may have functionally redundant paralogs; for example, PAPS can be synthesized by PAPSS1 and PAPSS2, both of which are expressed in GXRCas9 cells (**Supplementary Fig. 9a** and **Supplementary Table 3**). TPST2 and SLC35B2 are the dominant paralogs in both GXRCas9 cells and primary $CD4^+$ T cells (**Supplementary Fig. 9a**,**b** and **Supplementary Table 3**). Fourth, some genes facilitate, but are not essential for, HIV infection—for example, *LEDGF* biases integration to highly spliced transcription units but is not essential for integration[51,52]. Finally, host factors involved only in the latest stages of the HIV life cycle are not captured by our approach, as HIV tat, which drives our reporter, is expressed prior to unspliced viral RNA export, virion assembly, and budding[53].

The results presented here indicate the importance of the sulfation pathway in HIV infection, which was also highlighted recently by the development of eCD4-Ig, a synthetic fusion of CD4-Ig with a CCR5-mimetic sulfopeptide, which demonstrated higher neutralization capacity and breadth than any known broadly neutralizing antibody[54]. This therapeutic strategy required co-delivery of *TPST2* to mediate high levels of sulfation and effective neutralization.

TPST2 also sulfates key tyrosine residues on CXCR4 (ref. 55), the other major co-receptor for HIV, and these tyrosine residues on CXCR4 are known to mediate important interactions with HIV gp120 (refs. 56,57). Thus, inhibiting cellular protein sulfation may provide protection against CCR5-tropic, CXCR4-tropic, and dual-tropic HIV strains; this may be important given that therapies targeted specifically against CCR5 can drive a shift toward CXCR4 tropism *in vivo*[58,59]. Sulfation may also affect HIV in ways unrelated to entry (**Supplementary Note**).

We also determined the mechanism of *ALCAM* as an HDF. Aggregation of T cells has been demonstrated to be a hallmark of activated cells both *in vitro*[60] and *in vivo*[58,59]. HIV is known to spread more efficiently *in vitro* (up to several orders of magnitude) by direct cell–cell contacts than by cell-free transmission[61,62]. Our results demonstrate the importance of cell-to-cell transmission for effective HIV replication and may have implications for the clinical setting. Antiretroviral therapies and broadly neutralizing antibodies are known to have markedly less efficacy against cell-to-cell transmission[63,64]. Cell-to-cell transmission may also drive $CD4^+$ T cell decline *in vivo* through tissue inflammation and cell death by caspase-1-dependent pyroptosis[65]. Studies have also suggested that inflammation and viral replication in lymphoid tissues may continue even in individuals on antiretroviral therapy who have undetectable viral loads[66,67], possibly contributing to the long-term clinical risks and comorbidities observed in people living with HIV/AIDS. Therapies that disrupt interactions between a wide range of immune cell types have already been developed[68,69], and our results suggest that disrupting $CD4^+$ T cell aggregation may halt HIV spread *in vivo* (**Supplementary Note**).

Global use of combination antiretroviral therapy for HIV has saved tens of millions of lives and slowed the AIDS epidemic, but it has failed to prevent the emergence and spread of drug-resistant strains. Anti-HIV therapies that target host genes required by HIV may raise the barrier to drug resistance and potentially offer new interventional or curative strategies through gene therapy. Our study demonstrates that CRISPR-based genetic screens in physiologically relevant cells can specifically identify non-essential host proteins critical for viral infection, and applying this approach to other pandemic and epidemic viruses will allow robust and unbiased identification of novel therapeutic targets.

METHODS

Methods, including statements of data availability and any associated accession codes and references, are available in the online version of the paper.

Note: Any Supplementary Information and Source Data files are available in the online version of the paper.

ACKNOWLEDGMENTS

We would like to thank the Ragon Institute Virology, Imaging, and Flow Cytometry cores, as well as the Center for Computational and Integrative Biology (CCIB) DNA Core Facility at Massachusetts General Hospital. We would like to thank A. McKeon, P. Jani, N.W. Hughes, and B.X. Liu for superb technical assistance, and A. Brass, G. Gaiha, and J.S. Park for helpful discussions. pMM310 was obtained through the AIDS Reagent Program, Division of AIDS, NIAID, NIH from M. Miller (Merck Research Laboratories). All plasmid reagents generated in this study have been deposited in Addgene. This work was supported by the Howard Hughes Medical Institute (D.M.S. and B.D.W.), the National Institutes of Health (grants CA103866 (D.M.S.), F31 CA189437 (T.W.), P50 GM082250 (A.M. and N.J.K.), U19 AI106754 (J.F.H. and N.J.K.), and P01 AI090935 (N.J.K.)), the National Human Genome Research Institute

(grant 2U54HG003067-10; E.S.L.), the National Science Foundation (T.W.), the MIT Whitaker Health Sciences Fund (T.W.), the UCSF Sandler Fellowship (A.M.), a gift from J. Aronov (A.M.), the UCSF MPHD T32 Training Grant (J.F.H.), and the Deutsche Forschungsgemeinschaft (grant SCHU3020/2-1; K.S.). Support was also provided by NIH-funded Centers for AIDS Research (grant P30 AI027763, UCSF Center for AIDS Research (N.J.K.) and grant P30 AI060354, Harvard University Center for AIDS Research (B.D.W.)), which are supported by the following NIH co-funding and participating Institutes and Centers: NIAID, NCI, NICHD, NHLBI, NIDA, NIMH, NIA, FIC, and OAR. D.M.S. and B.D.W. are investigators of the Howard Hughes Medical Institute. R.J.P. is a Howard Hughes Medical Institute Research Fellow.

AUTHOR CONTRIBUTIONS

R.J.P., T.W., A.M., N.J.K., D.M.S., E.S.L., N.H., and B.D.W. designed research. R.J.P., T.W., D.K., J.F.H., P.L.-M., B.M., K.S., H.Y., and K.M.K. conducted experiments. W.G.-B. and A.P.-T. contributed methods and reagents. R.J.P., T.W., D.K., and J.F.H. analyzed data. R.J.P., T.W., N.H., and B.D.W. wrote the manuscript.

COMPETING FINANCIAL INTERESTS

The authors declare competing financial interests: details are available in the online version of the paper.

Reprints and permissions information is available online at http://www.nature.com/reprints/index.html.

© 2017 Nature America, Inc., part of Springer Nature. All rights reserved.

1. Friedrich, B.M. *et al.* Host factors mediating HIV-1 replication. *Virus Res.* **161**, 101–114 (2011).
2. Fätkenheuer, G. *et al.* Efficacy of short-term monotherapy with maraviroc, a new CCR5 antagonist, in patients infected with HIV-1. *Nat. Med.* **11**, 1170–1172 (2005).
3. Gulick, R.M. *et al.* Maraviroc for previously treated patients with R5 HIV-1 infection. *N. Engl. J. Med.* **359**, 1429–1441 (2008).
4. Tebas, P. *et al.* Gene editing of *CCR5* in autologous CD4 T cells of persons infected with HIV. *N. Engl. J. Med.* **370**, 901–910 (2014).
5. Hütter, G. *et al.* Long-term control of HIV by *CCR5* Δ32/Δ32 stem cell transplantation. *N. Engl. J. Med.* **360**, 692–698 (2009).
6. Glass, W.G. *et al.* CCR5 deficiency increases risk of symptomatic West Nile virus infection. *J. Exp. Med.* **203**, 35–40 (2006).
7. Srivastava, A., Pandey, S.N., Choudhuri, G. & Mittal, B. *CCR5*-Δ32 polymorphism: associated with gallbladder cancer susceptibility. *Scand. J. Immunol.* **67**, 516–522 (2008).
8. Singh, H., Sachan, R., Jain, M. & Mittal, B. *CCR5*-Δ32 polymorphism and susceptibility to cervical cancer: association with early stage of cervical cancer. *Oncol. Res.* **17**, 87–91 (2008).
9. Eri, R. *et al. CCR5*-Δ32 mutation is strongly associated with primary sclerosing cholangitis. *Genes Immun.* **5**, 444–450 (2004).
10. König, R. *et al.* Global analysis of host–pathogen interactions that regulate early-stage HIV-1 replication. *Cell* **135**, 49–60 (2008).
11. Brass, A.L. *et al.* Identification of host proteins required for HIV infection through a functional genomic screen. *Science* **319**, 921–926 (2008).
12. Zhou, H. *et al.* Genome-scale RNAi screen for host factors required for HIV replication. *Cell Host Microbe* **4**, 495–504 (2008).
13. Bassik, M.C. *et al.* Rapid creation and quantitative monitoring of high-coverage shRNA libraries. *Nat. Methods* **6**, 443–445 (2009).
14. Shao, D.D. *et al.* ATARiS: computational quantification of gene suppression phenotypes from multisample RNAi screens. *Genome Res.* **23**, 665–678 (2013).
15. Zhu, J. *et al.* Comprehensive identification of host modulators of HIV-1 replication using multiple orthologous RNAi reagents. *Cell Rep.* **9**, 752–766 (2014).
16. Wang, T., Wei, J.J., Sabatini, D.M. & Lander, E.S. Genetic screens in human cells using the CRISPR–Cas9 system. *Science* **343**, 80–84 (2014).
17. Shalem, O. *et al.* Genome-scale CRISPR–Cas9 knockout screening in human cells. *Science* **343**, 84–87 (2014).
18. Wang, T. *et al.* Identification and characterization of essential genes in the human genome. *Science* **350**, 1096–1101 (2015).
19. Hart, T. *et al.* High-resolution CRISPR screens reveal fitness genes and genotype-specific cancer liabilities. *Cell* **163**, 1515–1526 (2015).
20. Keele, B.F. *et al.* Identification and characterization of transmitted and early-founder virus envelopes in primary HIV-1 infection. *Proc. Natl. Acad. Sci. USA* **105**, 7552–7557 (2008).
21. Ochsenbauer, C. *et al.* Generation of transmitted and founder HIV-1 infectious molecular clones, and characterization of their replication capacity in CD4 T lymphocytes and monocyte-derived macrophages. *J. Virol.* **86**, 2715–2728 (2012).
22. Lai, M.M. Cellular factors in the transcription and replication of viral RNA genomes: a parallel to DNA-dependent RNA transcription. *Virology* **244**, 1–12 (1998).
23. Rolando, M. & Buchrieser, C. *Legionella pneumophila* type IV effectors hijack the transcription and translation machinery of the host cell. *Trends Cell Biol.* **24**, 771–778 (2014).
24. Egan, E.S. *et al.* Malaria. A forward genetic screen identifies erythrocyte CD55 as essential for *Plasmodium falciparum* invasion. *Science* **348**, 711–714 (2015).
25. Cavrois, M., De Noronha, C. & Greene, W.C. A sensitive and specific enzyme-based assay detecting HIV-1 virion fusion in primary T lymphocytes. *Nat. Biotechnol.* **20**, 1151–1154 (2002).
26. Kamiyama, S. *et al.* Molecular cloning and identification of 3′-phosphoadenosine 5′-phosphosulfate transporter. *J. Biol. Chem.* **278**, 25958–25963 (2003).
27. Beisswanger, R. *et al.* Existence of distinct tyrosylprotein sulfotransferase genes: molecular characterization of tyrosylprotein sulfotransferase 2. *Proc. Natl. Acad. Sci. USA* **95**, 11134–11139 (1998).
28. Baeuerle, P.A. & Huttner, W.B. Chlorate—a potent inhibitor of protein sulfation in intact cells. *Biochem. Biophys. Res. Commun.* **141**, 870–877 (1986).
29. Rosmarin, D.M. *et al.* Attachment of *Chlamydia trachomatis* L2 to host cells requires sulfation. *Proc. Natl. Acad. Sci. USA* **109**, 10059–10064 (2012).
30. Connell, B.J. & Lortat-Jacob, H. Human immunodeficiency virus and heparan sulfate: from attachment to entry inhibition. *Front. Immunol.* **4**, 385 (2013).
31. Farzan, M. *et al.* Tyrosine sulfation of the amino terminus of CCR5 facilitates HIV-1 entry. *Cell* **96**, 667–676 (1999).
32. Seibert, C., Cadene, M., Sanfiz, A., Chait, B.T. & Sakmar, T.P. Tyrosine sulfation of CCR5 N-terminal peptide by tyrosylprotein sulfotransferases 1 and 2 follows a discrete pattern and temporal sequence. *Proc. Natl. Acad. Sci. USA* **99**, 11031–11036 (2002).
33. Wu, L. *et al.* Interaction of chemokine receptor CCR5 with its ligands: multiple domains for HIV-1 gp120 binding and a single domain for chemokine binding. *J. Exp. Med.* **186**, 1373–1381 (1997).
34. Bowen, M.A. *et al.* Cloning, mapping, and characterization of activated leukocyte-cell adhesion molecule (ALCAM), a CD6 ligand. *J. Exp. Med.* **181**, 2213–2220 (1995).
35. Swart, G.W. Activated leukocyte cell adhesion molecule (CD166 or ALCAM): developmental and mechanistic aspects of cell clustering and cell migration. *Eur. J. Cell Biol.* **81**, 313–321 (2002).
36. Iolyeva, M. *et al.* Novel role for ALCAM in lymphatic network formation and function. *FASEB J.* **27**, 978–990 (2013).
37. Williams, D.W., Anastos, K., Morgello, S. & Berman, J.W. JAM-A and ALCAM are therapeutic targets to inhibit diapedesis across the BBB of $CD14^{+}CD16^{+}$ monocytes in HIV-infected individuals. *J. Leukoc. Biol.* **97**, 401–412 (2015).
38. Te Riet, J. *et al.* Dynamic coupling of ALCAM to the actin cortex strengthens cell adhesion to CD6. *J. Cell Sci.* **127**, 1595–1606 (2014).
39. van Kempen, L.C. *et al.* Molecular basis for the homophilic activated leukocyte cell adhesion molecule (ALCAM)–ALCAM interaction. *J. Biol. Chem.* **276**, 25783–25790 (2001).
40. Gartner, Z.J. & Bertozzi, C.R. Programmed assembly of 3-dimensional microtissues with defined cellular connectivity. *Proc. Natl. Acad. Sci. USA* **106**, 4606–4610 (2009).
41. Schumann, K. *et al.* Generation of knock-in primary human T cells using Cas9 ribonucleoproteins. *Proc. Natl. Acad. Sci. USA* **112**, 10437–10442 (2015).
42. Dustin, M.L. & Springer, T.A. T cell receptor cross-linking transiently stimulates adhesiveness through LFA-1. *Nature* **341**, 619–624 (1989).
43. Sabatos, C.A. *et al.* A synaptic basis for paracrine interleukin-2 signaling during homotypic T cell interaction. *Immunity* **29**, 238–248 (2008).
44. Zumwalde, N.A., Domae, E., Mescher, M.F. & Shimizu, Y. ICAM-1-dependent homotypic aggregates regulate CD8 T cell effector function and differentiation during T cell activation. *J. Immunol.* **191**, 3681–3693 (2013).
45. Kaelin, W.G. Jr. Use and abuse of RNAi to study mammalian gene function. *Science* **337**, 421–422 (2012).
46. Sasaki, N. *et al.* A mutation in *Tpst2*, encoding tyrosylprotein sulfotransferase, causes dwarfism associated with hypothyroidism. *Mol. Endocrinol.* **21**, 1713–1721 (2007).
47. Ding, Z.M. *et al.* Relative contribution of LFA-1 and Mac-1 to neutrophil adhesion and migration. *J. Immunol.* **163**, 5029–5038 (1999).
48. Ghosh, S., Chackerian, A.A., Parker, C.M., Ballantyne, C.M. & Behar, S.M. The LFA-1 adhesion molecule is required for protective immunity during pulmonary *Mycobacterium tuberculosis* infection. *J. Immunol.* **176**, 4914–4922 (2006).
49. Clément, A. *et al.* Regulation of zebrafish skeletogenesis by *ext2 (dackel)* and *papst1* (*pinscher*). *PLoS Genet.* **4**, e1000136 (2008).
50. Jäger, S. *et al.* Global landscape of HIV–human protein complexes. *Nature* **481**, 365–370 (2011).
51. Singh, P.K. *et al.* LEDGF (p75) interacts with mRNA splicing factors and targets HIV-1 integration to highly spliced genes. *Genes Dev.* **29**, 2287–2297 (2015).
52. Sowd, G.A. *et al.* A critical role for alternative polyadenylation factor CPSF6 in targeting HIV-1 integration to transcriptionally active chromatin. *Proc. Natl. Acad. Sci. USA* **113**, E1054–E1063 (2016).
53. Desfosses, Y. *et al.* Regulation of human immunodeficiency virus type 1 gene expression by clade-specific Tat proteins. *J. Virol.* **79**, 9180–9191 (2005).
54. Gardner, M.R. *et al.* AAV-expressed eCD4–Ig provides durable protection from multiple SHIV challenges. *Nature* **519**, 87–91 (2015).
55. Seibert, C. *et al.* Sequential tyrosine sulfation of CXCR4 by tyrosylprotein sulfotransferases. *Biochemistry* **47**, 11251–11262 (2008).
56. Kajumo, F., Thompson, D.A., Guo, Y. & Dragic, T. Entry of R5X4 and X4 human immunodeficiency virus type 1 strains is mediated by negatively charged and tyrosine residues in the amino-terminal domain and the second extracellular loop of CXCR4. *Virology* **271**, 240–247 (2000).
57. Lin, G., Baribaud, F., Romano, J., Doms, R.W. & Hoxie, J.A. Identification of gp120-binding sites on CXCR4 by using CD4-independent human immunodeficiency virus type 2 Env proteins. *J. Virol.* **77**, 931–942 (2003).

58. Ingulli, E., Mondino, A., Khoruts, A. & Jenkins, M.K. *In vivo* detection of dendritic cell antigen presentation to $CD4^+$ T cells. *J. Exp. Med.* **185**, 2133–2141 (1997).
59. Hommel, M. & Kyewski, B. Dynamic changes during the immune response in T cell–antigen-presenting cell clusters isolated from lymph nodes. *J. Exp. Med.* **197**, 269–280 (2003).
60. Inaba, K., Witmer, M.D. & Steinman, R.M. Clustering of dendritic cells, helper T lymphocytes, and histocompatible B cells during primary antibody responses *in vitro*. *J. Exp. Med.* **160**, 858–876 (1984).
61. Sourisseau, M., Sol-Foulon, N., Porrot, F., Blanchet, F. & Schwartz, O. Inefficient human immunodeficiency virus replication in mobile lymphocytes. *J. Virol.* **81**, 1000–1012 (2007).
62. Agosto, L.M., Uchil, P.D. & Mothes, W. HIV cell-to-cell transmission: effects on pathogenesis and antiretroviral therapy. *Trends Microbiol.* **23**, 289–295 (2015).
63. Chen, P., Hübner, W., Spinelli, M.A. & Chen, B.K. Predominant mode of human immunodeficiency virus transfer between T cells is mediated by sustained Env-dependent neutralization-resistant virological synapses. *J. Virol.* **81**, 12582–12595 (2007).
64. Sigal, A. *et al.* Cell-to-cell spread of HIV permits ongoing replication despite antiretroviral therapy. *Nature* **477**, 95–98 (2011).
65. Doitsh, G. *et al.* Abortive HIV infection mediates CD4 T cell depletion and inflammation in human lymphoid tissue. *Cell* **143**, 789–801 (2010).
66. Santangelo, P.J. *et al.* Whole-body immunoPET reveals active SIV dynamics in viremic and antiretroviral-therapy-treated macaques. *Nat. Methods* **12**, 427–432 (2015).
67. Lorenzo-Redondo, R. *et al.* Persistent HIV-1 replication maintains the tissue reservoir during therapy. *Nature* **530**, 51–56 (2016).
68. Yusuf-Makagiansar, H., Anderson, M.E., Yakovleva, T.V., Murray, J.S. & Siahaan, T.J. Inhibition of LFA-1–ICAM-1 and VLA-4–VCAM-1 as a therapeutic approach to inflammation and autoimmune diseases. *Med. Res. Rev.* **22**, 146–167 (2002).
69. Hourmant, M. *et al.* A randomized multicenter trial comparing leukocyte function-associated antigen 1 monoclonal antibody with rabbit antithymocyte globulin as induction treatment in first kidney transplantations. *Transplantation* **62**, 1565–1570 (1996).

© 2017 Nature America, Inc., part of Springer Nature. All rights reserved.

ONLINE METHODS

Cell culture. GXRCas9 cells were cultured in RPMI-1640 medium (Gibco) supplemented with 20% heat-inactivated FCS (Sigma), 10 mM HEPES (Gibco), 2 mM GlutaMAX (Gibco), and penicillin–streptomycin. HEK-293T cells were cultured in Iscove's modified Dulbecco's medium (IMDM) (Life Technologies) and supplemented with 20% heat-inactivated FCS (Sigma), 5 mM glutamine, and penicillin–streptomycin. Cell lines were verified to be mycoplasma negative by PCR.

Antibodies. The following antibodies were used throughout this study. From BioLegend: anti-CD4-APC clone RPA-T4, anti-ALCAM-PE clone 3A6, anti-CD11a-PE clone TS2/4, polyclonal anti-RELA(NF-κB p65), anti-CD18 clone TS1/18, and anti-CD45 clone HI30. From Becton Dickinson: anti-CCR5-BV421 clone 2D7, anti-CCR5-APC clone 2D7, and anti-sulfated-CCR5-BV786 clone 3A9. From Beckman Coulter: anti-HIV-gag (p24)-RD1 clone KC57. From Affymetrix: anti-ICAM1 clone RR1/1. From AbD Serotec: anti-CD11a clone 38. From Life Technologies: goat anti-mouse-IgG–Alexa Fluor 488. From Cell Signaling Technology: anti-RPS6 clone 5G10. From Tonbo Biosciences: anti-CD3 clone UCHT1 and anti-CD28 clone 28.2. All antibodies have been described and characterized in previous publications.

Flow cytometry. Cells were stained with antibodies in PBS + 2% FCS for 20 min at 4 °C and fixed with 4% paraformaldehyde. For intracellular staining for HIV gag, cells were fixed and permeabilized using Cytofix/Cytoperm (Becton Dickinson) prior to antibody staining. Data were acquired on a five-laser LSR Fortessa (Becton Dickinson) and analyzed using FlowJo software (TreeStar).

GXRCas9 cell line generation. CCRF-CEM cells stably transduced with *CCR5-hygR* and HIV-1 LTR-GFP, termed 'GXR', were generated previously[70]. GXR cells were transduced with a lentiviral construct expressing Cas9 and blasticidin deaminase (Cas9–bsd). Following 1 week of antibiotic selection, single, viable cells were sorted into 96-well plates by FACS. Subclones were analyzed by flow cytometry for expression of surface CD4, CCR5, and CXCR4, as well as GFP, before and after HIV infection. A subclone, termed GXRCas9, was selected for high receptor expression, low basal GFP expression, and high HIV-infection-induced GFP expression. Cas9 activity was confirmed by loss of surface CD4 expression in a majority of cells following lentiviral transduction with an sgRNA targeting *CD4*.

sgRNA library cloning and lentiviral production. A plasmid library containing 187,536 sgRNAs targeting 18,543 protein-coding human genes and 1,504 nontargeting control sgRNAs was synthesized as oligonucleotides (CustomArray) and cloned by Gibson assembly[71] as described previously[72] into a lentiviral sgRNA expression vector that did not contain Cas9 (ref. 73). The sgRNA sequences in this library include (i) the activity-optimized library generated previously[18] and (ii) 5,401 additional sgRNAs comprising 499 intergenic control sgRNAs and 4,902 sgRNAs targeting 497 additional protein-coding genes (**Supplementary Table 1**). Lentivirus was produced from HEK-293T cells as described previously[72].

Pooled genome-wide CRISPR screen. 240 million GXRCas9 cells were transduced with a lentiviral sgRNA pool to achieve an average 1,000-fold coverage of the library after selection. After 24 h, cells were selected with puromycin, and an initial pool of 80 million cells was collected for genomic DNA extraction using the QIAamp DNA Blood Maxi kit according to the manufacturer's instructions. One week later, 200 million puromycin-resistant cells were spin-infected with HIV-1 JR-CSF at an MOI of 0.025 in two six-well plates. After 3 weeks of culture, cells were re-infected with JR-CSF under the same conditions. After three additional weeks, 10 million viable, GFP^- cells were isolated by FACS and collected for genomic DNA. PCR, sequencing, and alignment to the sgRNA library were performed as previously described[16].

Screen analysis. Sequencing reads were aligned to the sgRNA library, and the abundance of each sgRNA was calculated. sgRNAs with fewer than 25 counts in the initial set were removed from downstream analyses. The $\log_2$–transformed fold change in abundance of each sgRNA was calculated for the infected and uninfected final population samples after adding 0.5 as a pseudocount. Gene-based CRISPR scores (CS) were defined as the fifth highest $\log_2$ fold change for all sgRNAs targeting a given gene or the average $\log_2$ fold change for all sgRNAs targeting a given gene.

Vector construction. Individual sgRNA constructs targeting *ALCAM*, *CCR5*, *RELA*, *SLC35B2*, and *TPST2*, as well as non-genic control sgRNAs, were cloned into pLenti-sgRNA[73] (sequences provided in **Supplementary Table 4**). For cell-free virus infection assays, all three control sgRNAs were used (sgCTRL-1 and sgCTRL-2 target noncoding regions of the genome, and sgCTRL-3 does not target a sequence in the genome). For all other experiments, sgCTRL-1 was used.

For cDNA expression vectors, a linearized lentiviral backbone was generated from LeGO-iC2 (Addgene, 27345)[74] by digestion with NheI and BsrGI. gBlocks (IDT) comprising the eukaryotic translation elongation factor 1 alpha 1 (*EEF1A1*)-short (EFS) promoter, the appropriate gene (*ALCAM*, *RAP2A*, *SLC35B2*, or *TPST2*), and p2A-E2Crimson were cloned into this backbone via Gibson assembly. Protein-coding sequences were codon optimized.

Clonal knockout and add-back cell line generation. GXRCas9 cells were transduced with sgRNAs targeting *SLC35B2* and *TPST2*. Single cells were isolated by FACS, and each of the resultant clonal populations was genotyped by deep sequencing and qPCR analysis. For add-back experiments, knockout lines were transduced with the appropriate cDNA expression constructs. E2-Crimson-positive cells were isolated by FACS.

qPCR analysis of knockout clones. Total RNA was extracted from 3×10^6 wild-type GXRCas9 cells and *TPST2*- and *SLC35B2*-knockout clones using the RNeasy Mini kit (Qiagen). First-strand cDNA synthesis was performed using 5 μg of total RNA with the SuperScript III First-Strand Synthesis System with oligo$(dT)_{20}$ (Invitrogen). qPCR was performed using FastStart Universal SYBR Green Real-Time PCR Master Mix (Roche) in a real-time PCR system (Applied Biosystems). Primers for *TPST2* and *SLC35B2* overlapped the sgRNA target to selectively amplify the wild-type cDNAs (sequences provided in **Supplementary Table 4**). Ribosomal protein S6 kinase A5 (*RPS6KA5*) expression was used as a reference normalization control, and expression levels were quantified by the ΔC_t method.

Cellular proliferation assays. ATP-based measurements of cellular proliferation were performed by plating 2,000 cells per well in 96-well plates. Six replicate wells were plated for each sample. At the initial time point or after 2 or 4 d, 50 μl of CellTiterGlo reagent (Promega) was added to each well and mixed for 5 min. Luminescence was measured on the Spectra Max M5 Luminometer (Molecular Devices).

Cell-free virus infection assays. GXRCas9 cells were plated in flat-bottomed 96-well plates at 100,000 cells/ml and spin-infected with medium only or HIV-1 JR-CSF at an MOI of 1 for 45 min at 800*g* and 25 °C. Three days later, cells were stained with propidium iodide (Life Technologies), and viable cells were counted using a combination flow cytometer and Coulter counter (MoxiFlow, Orflo Technologies). Cells were also analyzed by flow cytometry for GFP expression. The absolute number of viable, GFP^- cells in wells with HIV-infected cells was calculated and normalized to a corresponding medium-only control well.

Viral fusion assays. Entry of HIV virions into target cells was measured using a previously described assay[25]. Chimeric JR-CSF virions that contain the HIV Vpr protein fused to β-lactamase were generated by cotransfecting HEK-293T cells with a vector encoding JR-CSF and a plasmid encoding the *vpr* gene fused to the gene encoding β-lactamase (pMM310, NIH AIDS Reagent Program, 11444). Supernatant containing the virus was concentrated over a 20% sucrose solution in PBS by ultracentrifugation using a Sorvall WX100 ultracentrifuge (1.5 h, 150,000*g*, 4 °C). GXRCas9 cells were exposed to concentrated virus for 2 h at 37 °C. Cells were then washed and loaded with CCF2-AM (Invitrogen), a Förster resonance energy transfer (FRET) donor–acceptor pair linked by a β-lactam ring, in the presence of 1.8 mM probenicid (Sigma) for 2 h at room temperature. Cells were then washed and fixed. β-lactamase that is released into target cells after viral fusion cleaves the FRET acceptor (fluorescein) from CCF2, producing an emission shift that is analyzed by flow cytometry.

© 2017 Nature America, Inc., part of Springer Nature. All rights reserved.

doi:10.1038/ng.3741

Cellular sulfate depletion. Cells were cultured for 1 week in custom-made advanced RPMI-1640 medium (Life Technologies), with magnesium sulfate, zinc sulfate, and copper (II) sulfate replaced with their respective chloride salts, supplemented with FCS (Sigma), GlutaMAX (Gibco), penicillin–streptomycin, and 150 mM sodium chlorate (Sigma) as described previously[75]. Cells were then used in the viral fusion assay as described.

Heparinase treatment. GXRCas9 cells were washed three times in PBS and plated in a 96-well plate at 300,000 cells/well. 100 µl of *Bacteroides* heparinase II (New England BioLabs), diluted in PBS, was added to the well at a concentration of 2 U/ml, and cells were incubated at 37 °C for 1 h. Cells were then washed twice in PBS and used in the viral fusion assay as described.

Confocal microscopy. Cells were imaged on a Zeiss LSM 510 laser-scanning confocal microscope equipped with a 20× objective and far-red and diode (405-nm) lasers using ZEN software (Carl Zeiss). Images were acquired with optical sections at 0.33-µm intervals in the *z* axis. Slices were collapsed to single images using ImageJ software (NIH). For living cells, imaging was performed at 37 °C and 5% CO_2 in complete medium.

To image ALCAM, cells were loaded onto coverslips coated with poly(D-lysine) in 24-well plates. After 45 min at 37 °C, cells were fixed with 4% paraformaldehyde for 15 min at room temperature, permeabilized with 0.5% Triton for 15 min at room temperature, blocked with PBS + 3% BSA for 1 h at room temperature, and stained with anti-ALCAM antibody overnight at 4 °C. The coverslips were then stained with a secondary Alexa Fluor 488–conjugated anti-mouse-IgG antibody for 1 h at room temperature, washed, and mounted on slides using ProLong Gold Antifade Reagent containing DAPI (Life Technologies). Images were acquired with a 40× objective using the setup described above.

Cell-mixing study. GXRCas9 cells of the indicated genotype were fluorescently labeled using the CellTrace Far Red or Violet kit (Life Technologies). 50,000 each of violet- or red-labeled cells were co-cultured in 350 µl of complete medium in an eight-well Nunc Lab-Tek II Chamber Slide system (Thermo Scientific) and incubated for 1 h, followed by confocal microscopy analysis.

Cell-to-cell transmission assays. For donor cells, GXRCas9 cells of the indicated genotype were spin-infected with HIV-1 JR-CSF at an MOI of 1, except where indicated otherwise. After 4 h, GXRCas9 cells were washed extensively and resuspended in complete medium. For acceptor cells, GXRCas9 cells of the indicated genotype were fluorescently labeled using the CellTrace Far Red kit (Life Technologies). 40,000 each of donor and acceptor cells were co-cultured in 1.5 ml of complete medium in a 24-well plate. Where indicated, donor cells were placed in a 0.45-µm pore size Transwell (Corning). After 4 d, except where indicated otherwise, cells were counted and analyzed by flow cytometry, as in the cell-free virus infection assay.

For primary cells, the cell-to-cell transmission assay was modified as follows: donor cells were activated for 3 d using ImmunoCult Human CD3–CD28 T cell activator (StemCell Technologies), spin-infected at an MOI of 1 for 45 min at 800*g* and 25 °C, and cultured for 24 h prior to co-culture with acceptor cells. Acceptor cells were separately activated for 3 d and then fluorescently labeled prior to co-culture, as described above. After 2 d of co-culture, cells were stained and analyzed for intracellular HIV gag (p24) instead of GFP. For antibody blockade experiments, antibodies were added to donor and acceptor cells separately (10 µg/ml for anti-CD11a and anti-ICAM1, 20 µg/ml for anti-CD18, 10 µg/ml for anti-CD45) for 15 min at 37 °C prior to co-culture.

Oligonucleotide labeling of *ALCAM*-null GXRCas9 cells. 400 µg of 5′-thiol-modified oligonucleotides (sequences: $(ACTG)_5$ and $(CAGT)_5$) (IDT) dissolved in 10 mM Tris pH 7.5, 1 mM EDTA, and 10 mM Tris(2-carboxyethyl)phosphine (TCEP) (Thermo Scientific) was passed through a Centri-Spin 10 size-exclusion column (Princeton Separations) and exposed to 250 nmol of NHS-PEG6-maleimide (Thermo Scientific) in DMSO. This NHS-PEG_6-conjugated DNA was further purified through a Centri-Spin10 size-exclusion column that was pre-equilibrated with PBS. Concentration was determined using a NanoDrop 2000 spectrophotometer (Thermo Scientific).

200,000 GXRCas9 cells were washed three times with PBS and then resuspended in a 300 µM solution of NHS-PEG_6-conjugated DNA and incubated at room temperature for 1 h. Cells were washed three times with PBS + 1% FCS and used in downstream experiments.

Primary $CD4^+$ T cell isolation and culture. For donors 1 and 2, $CD4^+$ T cells were isolated directly from buffy coats obtained from healthy donors (Massachusetts General Hospital) using the EasySep Direct Human $CD4^+$ T cell Isolation kit (StemCell), according to the manufacturer's instructions. Isolated cells were cultured in X-VIVO 15 (Lonza) supplemented with 5% heat-inactivated human AB serum (Valley Biomedical), 55 µM β-mercaptoethanol (Gibco), and 10 mM *N*-acetyl-L-cysteine (Sigma).

For donors 3 and 4, PBMCs were isolated by Ficoll gradient centrifugation from whole blood that was collected from healthy donors (UCSF). $CD4^+$ T cells were then isolated using the EasySep Human $CD4^+$ T cell Enrichment kit (StemCell), according to the manufacturer's instructions. Isolated cells were cultured in complete RPMI medium, which consisted of RPMI-1640 (UCSF Cell Culture Facility (CCF)) supplemented with 5 mM HEPES, 2 mM glutamine, 50 µg/ml penicillin–streptomycin, 5 mM non-essential amino acids, 5 mM sodium pyruvate, and 10% FBS (Atlanta Biologicals).

Genetic editing of primary $CD4^+$ T cells. Cas9–RNPs were assembled as described previously[41]. Briefly, tracrRNA and crRNA (sequences provided in **Supplementary Table 4**) were hybridized in a 1:1 ratio at 37 °C for 30 min. Purified Cas9 protein was added in a 1:1 protein:RNA molar ratio, and the mixture was incubated at 37 °C for 15 min prior to electroporation.

For donors 1 and 2, primary $CD4^+$ T cells were activated using 10 µl of ImmunoCult Human CD3–CD28 T cell activator (StemCell Technologies) per milliliter of medium. After 3 d, 1 million cells were electroporated with 3 µl of Cas9–RNPs using Nucleocuvette strips in an Amaxa 4D-Nucleofector System X unit (P3 solution, program EO-115). Six days later, cells were re-activated using 2.5 µl of ImmunoCult reagent per milliliter of medium and cultured for three additional days prior to use in downstream assays including HIV challenge.

For donors 3 and 4, primary $CD4^+$ T cells were activated for 2 d with 5 µg/ml soluble anti-CD28 (Tonbo Biosceiences) on plates that were coated overnight with 10 µg/ml anti-CD3 (Tonbo Biosciences). Cells were electroporated with Cas9–RNPs as described above, except with 300,000 cells per condition. crRNA sequences are provided in **Supplementary Table 4**.

Assessing CRISPR editing efficiency by high-throughput sequencing. To extract DNA from GXRCas9 and primary $CD4^+$ cells, cells were incubated in a lysis solution (0.45% NP-40, 0.45% Tween-20, 200 µg/ml proteinase K) for 30 min at 55 °C and then at 95 °C for 10 min for protease inactivation. 1–5 µl of the solution was then used as a template for PCR amplification with MiSeq-compatible locus-specific primers using Takara Ex Taq (Clontech). The PCR products were cleaned and sequenced using an Illumina MiSeq.

Isolation of $CD11a^-$ primary $CD4^+$ T cells. For the CRISPR-based cell-to-cell transmission assay, primary T cells were edited using Cas9–RNPs targeting *ITGAL* (which encodes CD11a) as described above. Immediately prior to HIV infection for donors and co-culture for acceptors, cells were labeled with CD11a-PE antibody, incubated with MACS microbeads coated with anti-PE antibodies (Miltenyi Biotec), and run on an autoMACS Pro Cell Separator (Miltenyi Biotec) using the depl05 protocol for depletion of $CD11a^+$ cells. Purity was confirmed by flow cytometry.

Immunoblotting. Cells were rinsed once with ice-cold PBS and immediately lysed with Triton lysis buffer (1% Triton, 10 mM β-glycerol phosphate, 40 mM HEPES pH 7.4, 2.5 mM $MgCl_2$, and one tablet of EDTA-free protease inhibitor (Roche) per 25 ml of buffer). Cell lysates were cleared by centrifugation at 18,000*g* at 4 °C in a microcentrifuge for 15 min, separated on a NuPAGE Novex 12% Tris-glycine gel, and transferred to a polyvinylidene difluoride membrane (Millipore). Immunoblots were processed according to standard procedures, using primary antibodies (1:1,000 dilution) directed to RELA and the ribosomal protein RPS6, and analyzed using enhanced chemiluminescence

© 2017 Nature America, Inc., part of Springer Nature. All rights reserved.

with horseradish peroxidase (HRP)-conjugated anti-mouse and anti-rabbit secondary antibodies (1:10,000 dilution) (Santa Cruz Biotechnology).

RNA sequencing. Transcriptomic analysis was performed using the strand-specific RNA sequencing protocol described previously[18]. Briefly, total RNA was extracted using the RNeasy Mini kit (Qiagen). 5 µg of poly(A)-selected RNA was fragmented and dephosphorylated, after which an ssRNA adapter was then ligated. Reverse transcription was performed using a primer complementary to the RNA adaptor, after which a DNA adaptor was ligated onto the 3′ end of the resulting cDNA product. The library was then PCR amplified, cleaned, quantified using a TapeStation (Agilent), and sequenced on a HiSeq 2500 (Illumina). All primer sequences for this protocol have been previously described[18].

Statistical testing. In all cases, a two-sided Welch's *t* test, a modified Student's *t* test in which equal variance between samples is not assumed, was applied to assess statistical significance. A significance level (α) of 0.01 was set for all tests.

Data availability. All data generated or analyzed during this study are included in this published article (and its Supplementary Information files).

70. Brockman, M.A., Tanzi, G.O., Walker, B.D. & Allen, T.M. Use of a novel GFP reporter cell line to examine replication capacity of CXCR4- and CCR5-tropic HIV-1 by flow cytometry. *J. Virol. Methods* **131**, 134–142 (2006).
71. Gibson, D.G. *et al.* Enzymatic assembly of DNA molecules up to several hundred kilobases. *Nat. Methods* **6**, 343–345 (2009).
72. Wang, T., Lander, E.S. & Sabatini, D.M. Large-scale single guide RNA library construction and use for CRISPR–Cas9-based genetic screens. *Cold Spring Harb. Protoc.* **2016**, pdb.top086892 (2016).
73. McKinley, K.L. *et al.* The CENP–L–N complex forms a critical node in an integrated meshwork of interactions at the centromere–kinetochore interface. *Mol. Cell* **60**, 886–898 (2015).
74. Weber, K., Bartsch, U., Stocking, C. & Fehse, B. A multicolor panel of novel lentiviral 'gene ontology' (LeGO) vectors for functional gene analysis. *Mol. Ther.* **16**, 698–706 (2008).
75. Salzberger, W. *et al.* Influence of glycosylation inhibition on the binding of KIR3DL1 to HLA-B*57:01. *PLoS One* **10**, e0145324 (2015).

© 2017 Nature America, Inc., part of Springer Nature. All rights reserved.